

Distinguishing Unique Earthquakes with Overlapping Signals in Oklahoma

Paul Ogwari^{1*}, Jacob I. Walter¹, Xiaowei Chen², Andrew Thiel¹, Fernando Ferrer¹, and Isaac Woelfel¹

Abstract

During routine operations monitoring Oklahoma earthquakes, we found that certain earthquakes occurred closely both in space and time and had overlapping phases at the recording stations. Through further scrutiny and analysis, we determined that rather than being distinctly different earthquakes, some of the earthquakes exhibited multiphase arrivals and longer than expected coda due to unique ray paths that encounter impedance contrasts such as at the sedimentary rock-basement. Of course, some of these events truly were distinct events, which we term overlapping earthquakes, for which perceived coda duration overlaps and obscures the phase arrivals of the second event due to the source proximity in both time and space. We detail our classification scheme to separate the local earthquakes in Oklahoma as single, overlapping earthquakes, or those associated with multiphase arrivals. We forward model seismic wave propagation in a 2D crustal model and develop a methodology that utilizes waveform correlation to distinguish phases from overlapping earthquakes to those from crustal reverberations. Duration analysis shows a more elongated duration, qualitatively similar to the duration produced by overlapping earthquakes, at the sites where multiphase arrivals are observed.

Cite this article as Ogwari, P., J. I. Walter, X. Chen, A. Thiel, F. Ferrer, and I. Woelfel (2022). Distinguishing Unique Earthquakes with Overlapping Signals in Oklahoma, *Seismol. Res. Lett.* **XX**, 1–12, doi: [10.1785/0220220065](https://doi.org/10.1785/0220220065).

[Supplemental Material](#)

Background

Oklahoma experienced four large earthquakes ($M_w > 5$) over the past 15 yr alongside the unprecedented rise of seismicity rates in the oil and gas producing regions of the state. Much of the activity in the last 8 yr corresponds to a broad area in north-central Oklahoma where an increased seismicity rate has been attributed to the injection of wastewater from the oil production process into the Arbuckle Group, with most of the seismicity occurring in the Precambrian basement (e.g., Ellsworth, 2013; Yeck *et al.*, 2017). A more recent trend of increased seismic activity has emerged in the gas production region of SCOOP and STACK area (Fig. 1), where most of the seismicity is related to the hydraulic fracturing process (Skoumal *et al.*, 2018; Shemeta *et al.*, 2019). The area has been designated as the SCOOP and STACK Area of Interest (SCOOP and STACK AOI on Fig. 1) by the Oklahoma Corporation Commission (OCC) following an increase in seismicity rate starting December 2016, commonly coincident with hydraulic fracture stimulation times. Generally, the OCC designates an AOI to a region where higher priorities are assigned to regulate the anthropogenic factors linked to the increased rate of seismicity. Within the SCOOP/STACK area, the OCC applies a spotlight protocol (OCC, 2016) to mitigate triggered seismicity during the hydraulic fracturing process (Holland, 2013; Skoumal *et al.*, 2018).

Starting in March 2019, concurrent with a shift to the SeisComP3 monitoring software (Walter *et al.*, 2020), Oklahoma Geological Survey (OGS) analysts began identifying pairs of earthquakes that occur closely both in space and time. Some of the events occur with such a short difference in origin time that the coda appears elongated, when observed at a single station. Although these are readily identifiable as overlapping earthquakes, we have observed an emerging trend of multiphase arrivals associated with low magnitude earthquakes ($M_L < 3$) occurring on some active fault sections within the SCOOP and STACK area. These phases are more prominent and more easily identifiable within near-source epicentral distances (<75 km) on the horizontal components of the recording seismographs. Most of the seismicity in this area is composed of earthquakes with magnitudes less than M_L 3.0.

We report our efforts to identify and classify the unique earthquakes occurring between January 2019 and December 2020 into different groups based on the recorded and

1. Oklahoma Geological Survey, Sarkeys Energy Center, University of Oklahoma, Norman, Oklahoma, U.S.A., <https://orcid.org/0000-0001-6234-6910> (PO); <https://orcid.org/0000-0001-7127-9422> (JWW); 2. School of Geosciences, Sarkeys Energy Center, University of Oklahoma, Norman, Oklahoma, U.S.A., <https://orcid.org/0000-0001-6362-3297> (XC)

*Corresponding author: pogwari@ou.edu

© Seismological Society of America

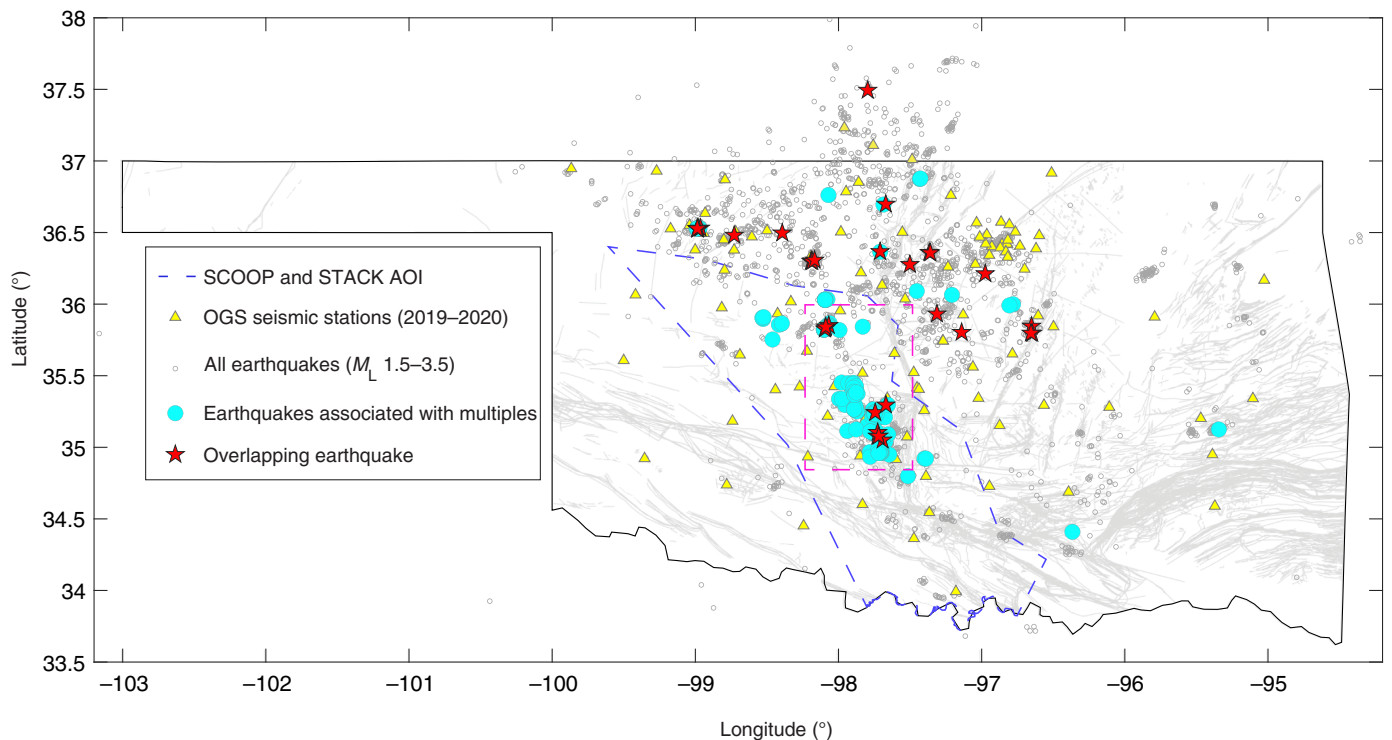


Figure 1. A map of earthquakes and Oklahoma Geological Survey (OGS) operating seismic stations (triangles) in Oklahoma for the period between January 2019 and December 2020. The earthquakes are grouped as identified overlapping earthquakes (red pentagrams), those associated with multiphase arrivals (cyan filled circles) and all other earthquakes (gray open dots) recorded within the period. The blue dashed line marks the SCOOP and STACK area. The pink dashed rectangle marks the area later selected to analyze ground-motion duration. In the background (gray lines) are mapped faults in Oklahoma. The color version of this figure is available only in the electronic edition.

observable phases at different stations. By virtue of the definition of the closely occurring overlapping events, we demonstrate the possibility of missed earthquakes due to obscured phases by apparent shadow zones. We develop a methodology that utilizes waveform correlation to distinguish overlapping events' phases from secondary phases originating from crustal reverberations and converted phases, here in referred to multiphase arrivals. The analysis follows three stages. First, we model synthetic waveforms and perform waveform correlation between modeled S -wave signal and the subsequent phases within the same waveform record, then identify the distinguishing elements between overlapping earthquakes and multiphase arrivals. Second, based on analysis of the forward model, we apply waveform correlation on a set of overlapping earthquakes to establish a statistical measure that defines them. Finally, based on the results from the overlapping earthquakes, we apply waveform correlation on a set of earthquakes with associated multiphase arrivals to search for possible overlapping earthquakes within them. We later spatially characterize the events with recorded multiphase arrivals. Based on results from detailed waveform analyses of the overlapping earthquakes, we apply an appropriate spatiotemporal window to detect overlapping earthquakes from the OGS catalog starting in 2010. Finally, we evaluate the significance of the unique earthquakes on the recorded ground-motion duration.

Earthquake Classification

“Regular” events that have simple P - and S -phase arrivals as the only observable phases at the recording seismic stations compose the vast majority of earthquakes detected on the state

seismic network (Walter *et al.*, 2020), which is part of the Advanced National Seismic System; we herein refer to regular earthquakes as singles. This article focuses on the classification of two additional special groups based on the observed waveform signatures at different stations. The first group is composed of event pairs we term as “overlapping earthquakes” that are spatially and temporarily close enough that we observe overlap of the respective signals. The second group is composed of earthquakes that exhibit multiphase arrivals observed on a single seismogram in addition to or obscuring the usual P and S phases when the event is recorded at regional distances. Although the hallmark identifier is the presence of multiphase arrivals on a single seismograph, usually we can observe the phenomena on several seismographs at different stations during routine processing of the earthquake catalog. Some of these extra phases originate from either crustal reverberations or are P - S and S - P converted phases. In some cases, these phases may not be easily distinguishable from convoluted overlapping body waves by visual observation and require a set of

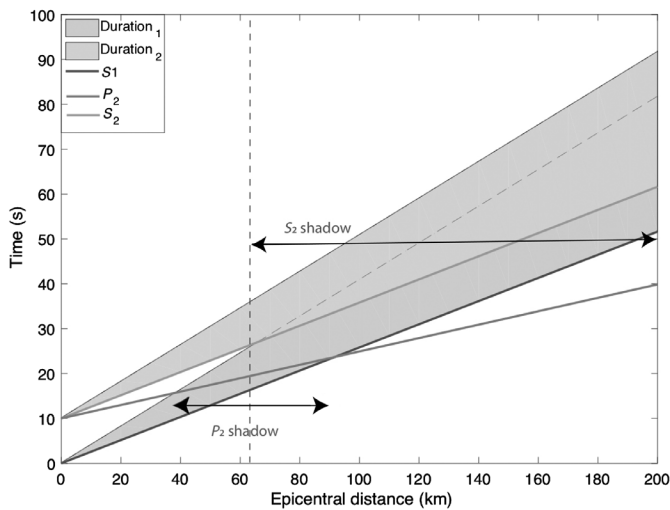


Figure 2. An illustration of the significant duration window of two earthquakes with an origin time separation of 10 s. The arrows mark the shadow zones for the P_2 and S_2 wave phases for the second earthquake.

algorithmic techniques for definitive classification. We propose that waveform variation within the coda can help distinguish the multiphase arrivals from a set of possible overlapping earthquakes. Figure 1 shows the spatial distribution of the three groups of earthquakes of magnitude M_L 1.5–3.5 for the 2019–2020 period. During that period, we identified 34 pairs of overlapping earthquakes and 128 earthquakes that are associated with multiphase arrivals that we will analyze to clearly distinguish multiphase arrivals from crustal reverberation and those from possible convolved overlapping earthquakes. Finally, during the study period, 4000 singles occurred.

Overlapping Events S – P Time Shadow Zone

When the seismic signals from an overlapping pair of earthquakes in close spatiotemporal proximity pass by a receiver station, phase identification can be obscured by the coda of the first-arriving event body waves. Identifying the second event can be difficult for nearly equally-sized earthquakes (e.g., M 2.0 and 2.2 separated by 2 s). In general, for a colocated pair of events, the separation time between the pairs of P arrivals and, by extension, the S arrivals at a particular station is equal to the difference in origin time. Although the separation time between similar phase-pairs remains constant with increase in epicentral distance, the S – P and duration increases with distance such that the P and S arrivals of the second event are overlapping with the coda of the first event at a later time and distance. In the case in which the second event is smaller than the preceding event, the convolved phases are shadowed by the coda of the earlier event and thereby become difficult to identify.

We present an example demonstrating how this window may be shadowing and limiting the phase picking and, by extension, the location of overlapping earthquakes in the region. We express the shadow zone or window by simulating the significant duration (SD) estimate from the [Kempton and Stewart \(2005\)](#) duration derived from Brune’s earthquake source model ([Brune, 1970](#)). The SD is defined as:

$$\ln \text{SD} = \ln \left[\frac{\left(\frac{\exp(b_1 + b_2(M-6))}{10^{1.5M+16.05}} \right)^{\frac{1}{3}}}{4.9 \times 10^6 \beta} + c_2 r + c_1 s \right], \quad (1)$$

in which b_1 and b_2 are coefficients obtained from regression of stress drop in relation to magnitude M , whereas c_1 and c_2 are coefficients correcting for site and epicentral distance, respectively. For our purposes, we approximate the $\text{SD}_{v_{5-75}}$ eclipsing 5%–75% of the energy for a magnitude M 2 earthquake. For $\text{SD}_{v_{5-75}}$, b_1 , b_2 , c_1 , and c_2 are 5.46, 0, 1.17, and 0.1, respectively, with a shear-wave velocity β of 3.2 km/s. The site factor s is assigned a unit value and r is the epicentral distance.

We later estimate the ground-motion duration based on the Arias intensity, I_A , ([Arias, 1970](#)) by determining the SD on horizontal component velocity seismograms filtered between 1 and 15 Hz. We determine the duration using Husid plots that are the cumulative build-up of the Arias intensity and consider the time interval between 5% and 75% of I_A to overcome the high background noise at some of the stations in the network. Figure 2 shows the estimated durations of two colocated earthquakes that occur within 10 s time difference. We assume the bulk of the energy on the horizontal components is within the S -wave signal, as observed in most of the seismograms, hence most of the 5%–75% duration is appended on the period following each of the S -wave arrivals.

Figure 3 shows a pair of overlapping earthquakes of magnitude M_L 2.5 recorded at 20.3 km (SC19), 24.5 km (SC18), 40 km (CRES), and 92 km (FW10). At station SC19, the body-wave signals for the two earthquakes are clearly identifiable. However, at SC18 the P phase of the second earthquake falls within the S -wave coda of the first event such that recognition of the second earthquake is only clear from the seismogram recorded at station SC19. At a further epicentral distance, CRES falls within the P -wave shadow zone and the second P wave is no longer recognizable. Beyond the P -wave shadow zone, the P arrival for the second event re-emerges and is observable but the S -wave arrival is obscured in the S -wave signal of the first event.

Distinguishing Multiphase Arrivals and Overlapping Earthquakes Numerical modeling

The presence of multiphase arrivals and overlapping earthquakes in the same spatiotemporal subspace (e.g., Fig. 1) presents uncertainty in classification, especially for stations at

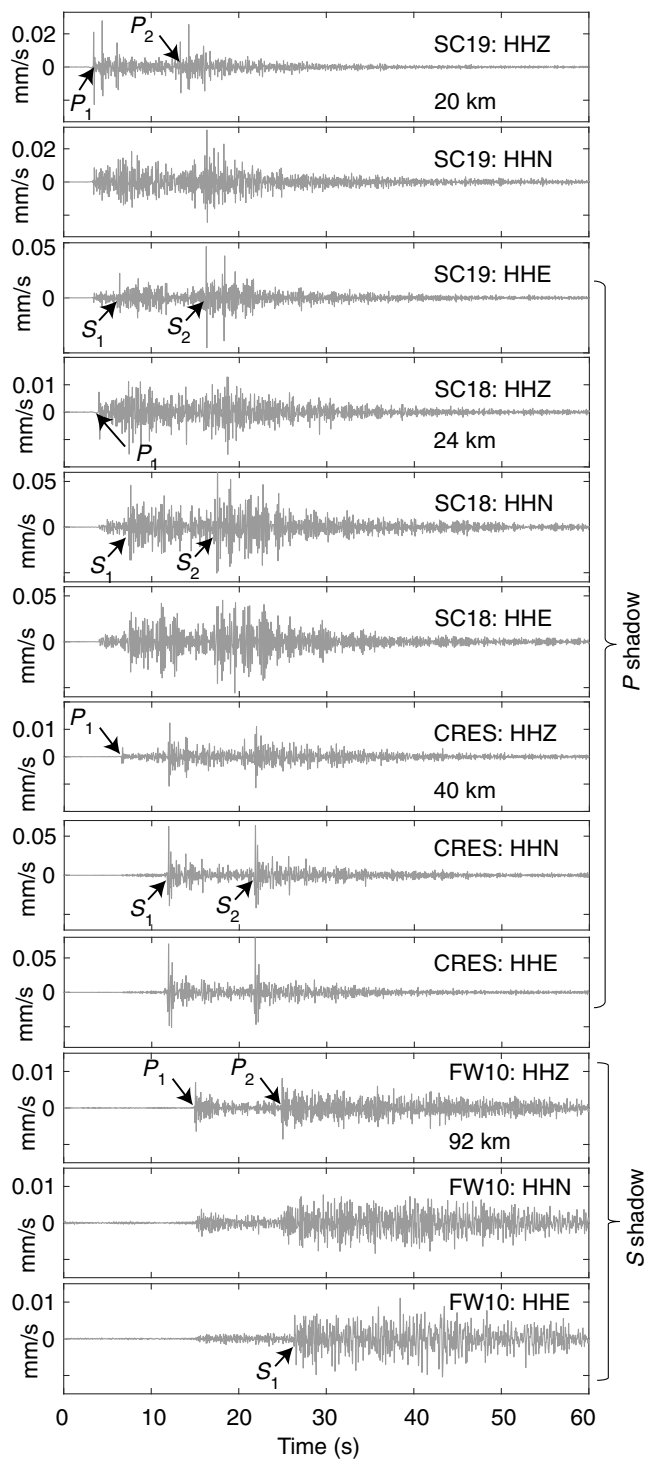


Figure 3. A set of overlapping earthquakes of magnitude M_L 2.5 with overlapping signal over wide spectrum of epicentral distance. P_1 and S_1 are the P and S phase of the first event, whereas P_2 and S_2 are the P and S phases for the second event respectively.

further distance from the epicenters. In this section, we forward model seismic wave propagation that exhibits crustal reverberation, then simulate multiple event waveform interference. We utilize *sofi2D* software (Bohlen and Thomas 2002) to compute a

numerical forward model of the seismic wave propagation in a 2D crustal model. We structure the model velocity based on measured P -wave velocity from Toth *et al.* (2012) for central Oklahoma and a V_P/V_S ratio of 1.734. In the model, we assume a frequency-independent Q factor of 1200 in the basement and 1000 in the sedimentary material based on central North American region values derived by Dreiling *et al.* (2016). The 2D finite-difference numerical model does not solve for SH waves, hence the Love waves are not considered in the model. We structure the total extent of the crustal model to 80 km in length and 10 km in depth to show wave propagation at relatively long epicentral distances for relatively small local events. In the model, the spatial resolution is 20 m. The model left, right, and lower boundaries have 50-node-thick damping boundaries that absorb 8.5% of wave energy per node, whereas the upper boundary is a free-reflecting surface. We set the numerical time-step interval to 1 ms for a total model run time of 30 s. The earthquake sources are point shear dislocations, positioned at 20 km from the left edge of the model, that radiate Fuchs-Müller source time function at a center frequency of 7.5 Hz. We model focal depth at varying depth intervals corresponding with different stratigraphic layers to test the excitation of crustal reverberations and record the synthetic seismographs on the grid at every 4 km interval (Fig. S1, available in the supplemental material to this article).

The simulation indicates the crustal reverberations are best produced when the focal depth is within 0.5 km below the top of the basement, which is at 4.3 km depth in the model. The reverberations are most clear within 16–30 km epicentral distance range and are characterized by lower frequencies relative to the S -wave signal (Fig. 4). The signal length of the S wave and the reverberations achieved at the ~ 20 km receiver in the forward model is relatively equivalent to what we observe in field recorded waveforms band-passed between 1 and 5 Hz. Based on the subtle difference in frequency content (Fig. S2), we perform waveform correlation between the S -wave signal and the reverberations to test the viability of applying correlation function to differentiate a secondary S wave from the crustal reverberation. We select the ~ 20 km receiver waveform synthetics for two earthquake sources separated by two seconds to produce overlapping phase arrivals. In this case, the S -wave signal of the second event overlaps with the reverberations recorded alongside the first event. We then test different S -wave signal window lengths by performing sliding window cross correlation to check for the window that provides the highest correlation between two S -wave phases and lower correlation between the first S -wave signal and crustal reverberation. We start with a window that ellipse 0.5 s before S wave and 0.5 s after, then make increments of 0.5 s after S phase up to 3.0 s (Fig. S3). A window beyond 3 s after S phase is not suitable because it samples the reverberations we are trying to discern. We find from the correlation analysis that a suitable S -wave signal window eclipsing 0.5 s before the S phase, and

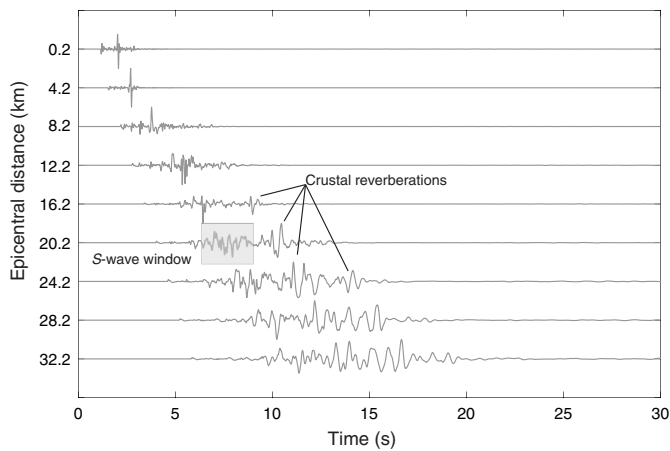


Figure 4. A set of synthetic SV waveforms for a single source depth of 4.5 km. Multiphase arrivals from crustal reverberation appear within the 16–30 km epicentral distance. The shaded rectangle illustrates the S-wave window used to perform waveform correlation.

2.0 s after, provides the highest correlation factor ($CC = 0.7$) at the second S-wave interval with a lower correlation factor for the next high correlating time interval. We find shorter S-wave windows simplify the signal and thereby produce false positives with higher correlation factors at other time intervals than the desired second S-wave interval. We note that the derived correlation window produces a $CC < 0.5$ when applied to the single event waveform (Fig. S3). This derived window is adequate to distinguish an S-wave signal from crustal reverberations in the event of overlapping signal from two earthquakes.

Field waveform correlation

We apply waveform cross correlation on a set of overlapping events to establish a statistical measure by which we can search for possible overlapping earthquakes in a dataset of multiphase arrivals. For each pair of overlapping earthquakes, we obtain waveforms from Incorporated Research Institutions for Seismology Data Management Center and arrival time picks from the OGS database, and apply a band-pass filter of 1–10 Hz to all waveforms. For each recording station, we choose an S-wave signal window eclipsing 0.5 s before the S phase and 2.0 s after of the first event of the overlapping earthquakes, as established in the analysis of the synthetics, and cross correlate with waveform windowed between 90 s before and after the selected S phase to allow for random selection of either of the two events in a pair, and a window long enough to accommodate for varying origin time-difference within pairs of identified overlapping earthquakes. We perform the cross correlation using the GISMO package (Reyes and West, 2011) for all stations recording at least the first event of the pair, then analyze the correlation coefficient (CC) and the correlation lag time of the coefficients.

Analysis of the CC indicates the correlation between the S-wave signals of the event pair varies across the stations and for different pairs of events. We define “correlation lag” as the time delay between the correlating S-phase arrival time and the highest coefficient time interval (Fig. 5), and define a “correlation lag cluster” if the variance of the correlation lag from all available stations of one event pair is less than 0.2 s. The threshold of 0.2 s is based on the average minimum hypocentral distance within the analyzed dataset, which is approximately 8 km. The S-wave travel-time variation for earthquakes located within 1 km radius subspace is less than 1 s at 8 km hypocentral distance and gets much smaller for larger hypocentral distances. Figure 6a shows the distribution of the number of stations for each overlapping event-pair that form a correlation lag cluster. The analysis produces only one cluster for each overlapping event-pair. From the distribution we establish a minimum of four stations as the threshold by which the temporal clustering of the lag time can be applied to identify a pair of overlapping earthquakes. Figure 6b shows the distribution of the CC for each cluster composed of at least four stations. Based on the analysis we set a CC of 0.6 as the minimum threshold to search for possible overlapping S-wave signals in the set of multiphase signals.

We apply the earlier correlation criteria achieved from analysis of overlapping earthquakes to a set of earthquakes with observable phases beyond the S-phase arrival and distinguish the overlapping earthquake signal from crustal reverberations. We select a similar S-wave signal window, as discussed previously, on the filtered waveform and perform cross correlation on the waveform windowed between 1.5 s before and 10.0 s after S-wave arrival. The band-pass filter of 1–10 Hz applied to this set of earthquake waveform is similar to the one applied on the singles. We select the correlation window to search for overlapping earthquakes based on the observed signal in the timeseries. The multiphase arrivals occur within the first 10 s after the S-phase arrival, beyond which is a decaying coda. We finally apply the same criteria for correlation lag clustering of at least four stations, as applied before, and search for possible overlapping earthquakes within the set of multiphase arrivals. The analysis identifies three sets of overlapping events from a set of 128 events producing multiphase arrivals through waveform propagation (Fig. S4).

Characterizing crustal reverberations

We further analyze the events producing multiphases using waveform correlation. In this instance, we use waveform cross correlation to group events into similar event clusters that have a minimum CC of 0.6 from four stations for P-wave and S-wave separately and each cluster is composed of a minimum of four events. We pre-cut waveforms 1.5 s before and 3.5 s after picked P-wave arrival on vertical channels, and 1.5 s before and 5.0 s after picked S-wave arrival on horizontal channels. A band-pass filter of 1–10 Hz is applied to all windowed

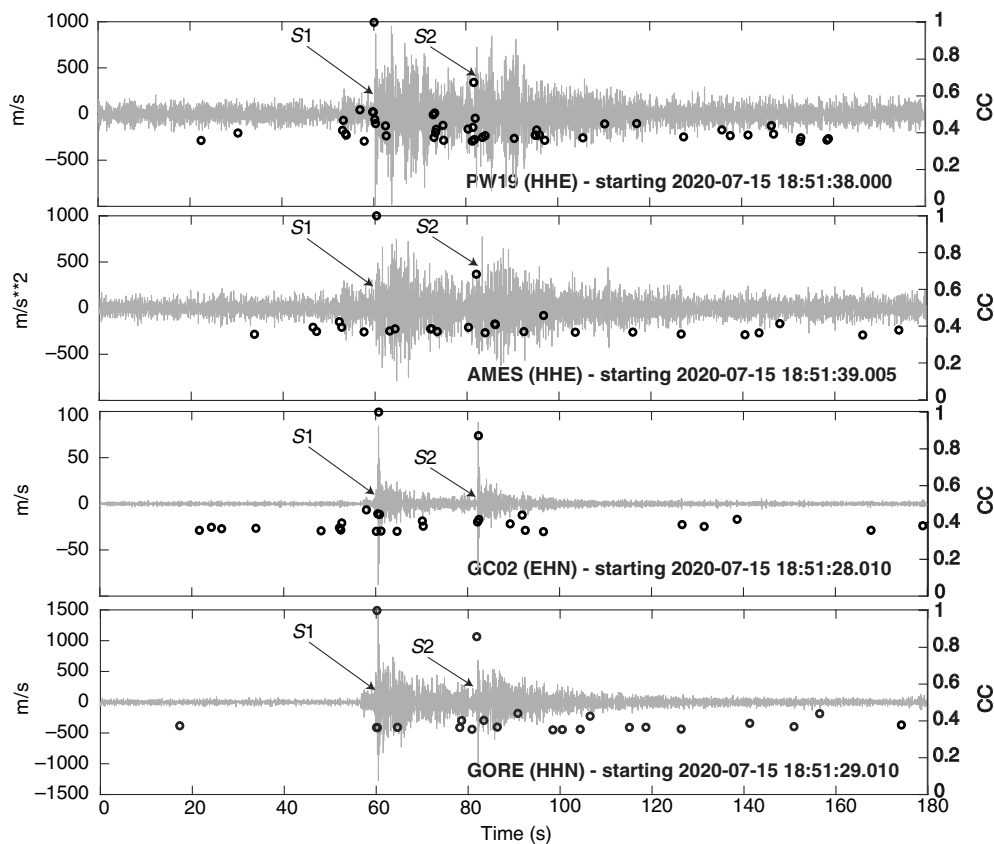


Figure 5. A set of overlapping earthquakes with high correlation ($CC > 0.6$) at each station between the first event S wave (S_1) and the second event S wave (S_2). The correlation lag between the master snippet time interval (S_1) and the next highest correlation time interval is approximately 20 s across the recording stations, thereby forming a cluster of correlation lag time.

waveforms, then waveform cross correlation and clustering is performed. Figure 7 is an example of the subclustering around the S -wave phase showing multiphase arrivals at stations MOOR, ARCA, CHOK, and PERK. The analysis results in nine clusters of earthquakes that are made up of at least four earthquakes in each cluster. There are 49 earthquakes forming the nine clusters from the analyzed 129 events. These emerge as closely located earthquakes, in each cluster, that seem to have similar ray paths to the recording stations. In each cluster, for each station, the clustering waveforms are similar with equal time difference between the S -phase arrival and the subsequent multiphase arrivals. However, when comparing some clusters that overlap in space or are closely located, for common stations, the time difference between the S -phase and multiphase arrivals is not equal. In some cases, some stations exhibit more sets of multiphase arrivals compared to other stations recording the same set of earthquakes (Fig. 7).

Elongated ground-motion duration

Overlapping and multiphase events create a longer coda than otherwise expected. To quantify this elongation, we evaluate a

subset of the earthquakes of the M_L 1.5–2.5 magnitude range based on the availability of events in the three groups. We further select a small study area (Fig. 1) to minimize the hypocentral distance variation across the recording stations, thereby minimizing the possible influence of varying signal paths and provide a direct comparison of the three earthquake groups at each station without variation of the epicentral distance.

We calculated the duration–distance distribution of the SD from the two defined special groups and “single” events (Fig. 8). A comparison of duration from the three groups shows an increasing duration with increase in hypocentral distance for all the groups as expected in the first 100 km epicentral distance, then the duration from the three groups starts to decrease at epicentral distances beyond 100 km due to signal attenuation at stations located at further epicentral distances. The overlapping

earthquakes exhibit the longest duration due to the overlapping ground motion from the event-pairs. The longer SD within the overlapping earthquakes ($SD > 60$ s) corresponds to a larger time interval between events forming a pair of overlapping earthquakes.

Between 20 and 100 km, the SD for single events suggests a less wide scatter relative to the special event types. The earthquakes associated with multiphase arrivals produce a duration equivalent to those produced by singles on some stations but a more elongated duration on others. This anomalously longer duration produced by some earthquakes associated with multiphase arrivals can be, in some cases, equivalent to the duration produced by some of the overlapping earthquakes.

Discussion

Overlapping earthquakes

Within seismological nomenclature, a doublet or multiplet is usually defined as a pair or a group of earthquakes with similar waveforms, though not necessarily at close origin times, with stress release originating from the same fracture (Moriya *et al.*, 2002). Such events of similar waveforms occur in nearly the

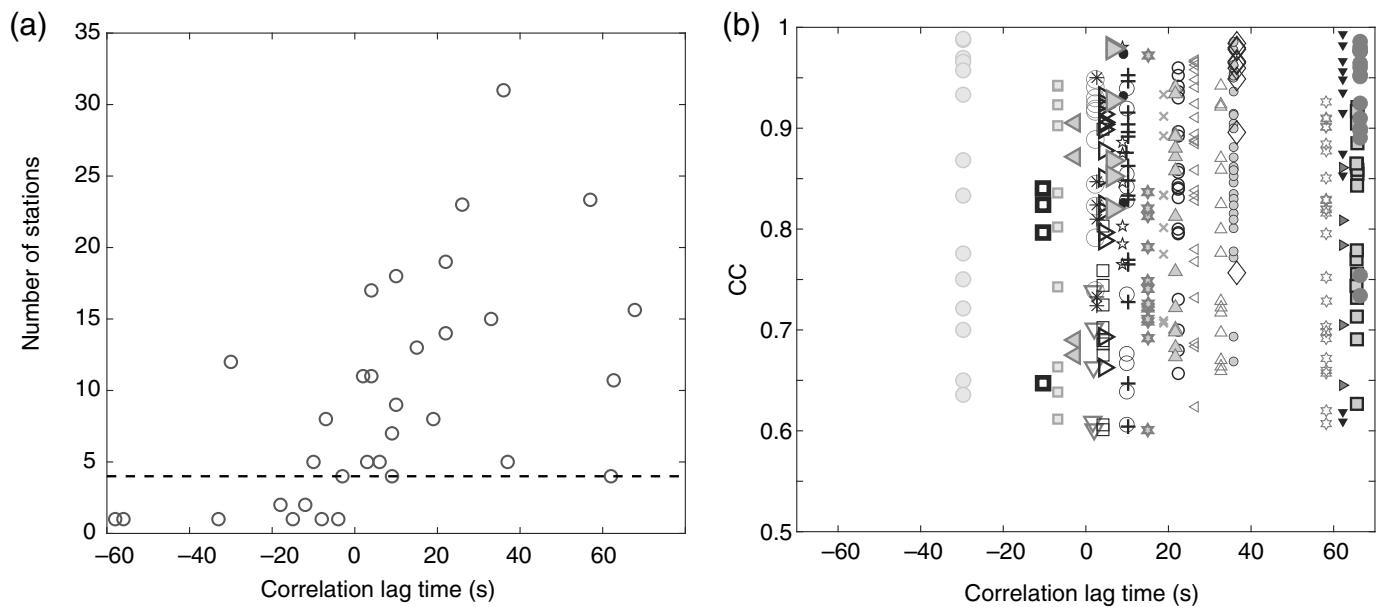


Figure 6. (a) The distribution of temporal cluster of the correlation lag versus the number of stations in each cluster and (b) the distribution of the CC in the cluster composed of at least four stations. We set the threshold for detecting overlapping

earthquakes to four stations (dashed line in panel a) and establish the minimum CC threshold as 0.6 to detect a pair of overlapping earthquakes described in panel (b). The different symbols in panel (b) are used to distinguish different event-pair clusters.

same focal point and share a similar source time function and ray path, but their magnitude need not be the equivalent (Poupinet *et al.*, 1985; Lees, 1998). In this study, we consider earthquakes that do not necessarily originate from the same fault patch or with similar waveforms but rather events that

are spatially and temporarily close enough that we observe overlap of the respective signals within 100 km epicentral distance. Given the small size of the events and overlapping coda, it can be difficult to determine a focal mechanism for the overlapping earthquakes.

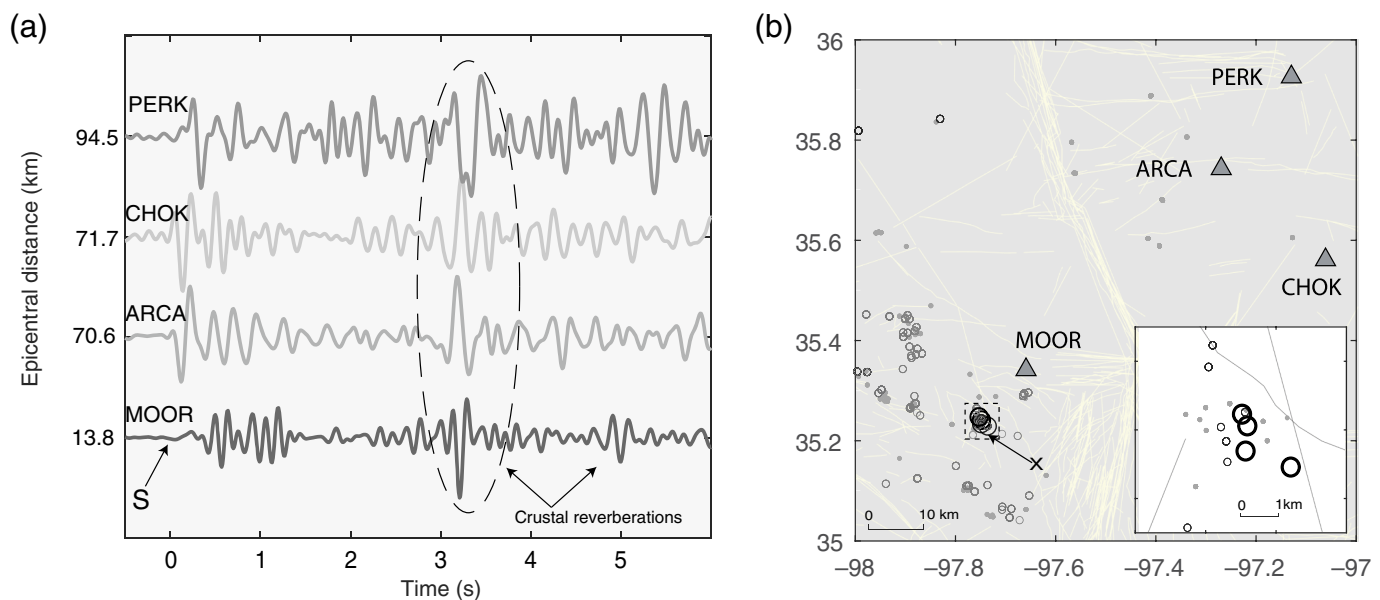


Figure 7. (a) Station stacked correlated waveforms at varying epicentral distance showing the *S* wave and crustal reverberation from clustered earthquakes associated with multiphase arrivals (X in panel b) across a subset of the seismic stations (triangles in panel b). (b) Spatially compact clustered earthquakes associated

with the multi-phase arrivals (open gray circles) and singles (gray dots). The inset shows the zoom-in area (dotted square in panel b) showing collocated earthquakes with varying characteristics. The color version of this figure is available only in the electronic edition.

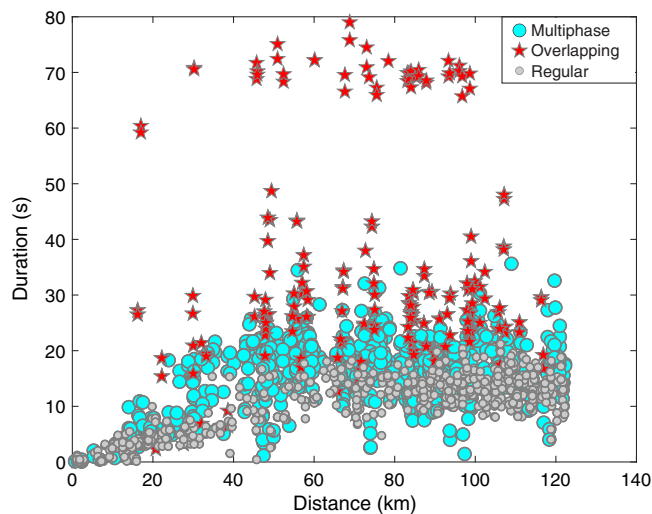


Figure 8. Significant duration earthquakes recorded within 120 km hypocentral distance. The overlapping earthquakes are the red pentagram, cyan large circles are earthquakes associated with multiphase arrivals, and gray small circles are singles. The magnitude range for the singles and events associated with multi-phase arrivals is M_L 2.5–3.5, whereas the range for the overlapping earthquakes is M_L 2.0–2.5. The color version of this figure is available only in the electronic edition.

Although the bulk of the article focuses on a time period since 2019, there are likely other observations of overlapping earthquakes in earlier records, and they may occur in other places when the seismicity was higher. By applying a 12 s and 2.5 km spatiotemporal window, derived from statistics of analyzed overlapping earthquakes (Fig. 9), on the OGS catalog and searching for overlapping earthquakes starting January 2010 through September 2020, we find 73 pairs with about 62% occurring after 2018. Notably, 19 pairs accounting for 26% of the record occur between early 2015 and mid-2017, which coincides with the period of the highest historical seismicity rate (~ 3 M 3.0 or greater earthquakes per day), during which the $M_w > 5$ Fairview, Pawnee, and Cushing earthquakes occurred.

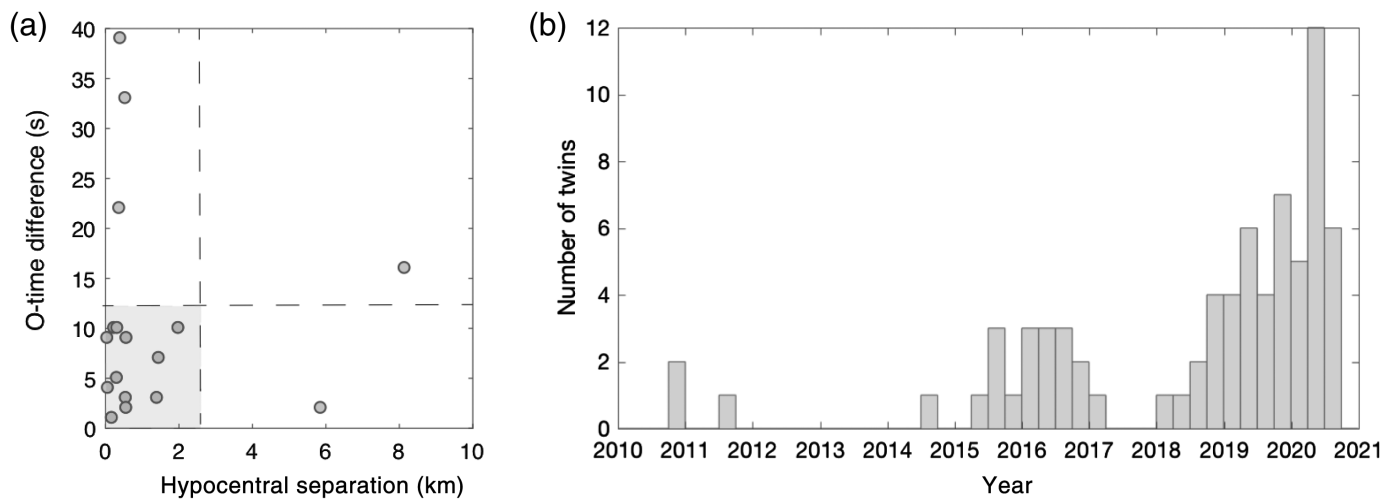
Earthquake detection and location in Oklahoma has improved over time since 2010 due to improved seismic network coverage over the years (Walter *et al.*, 2020). Our initial identification of overlapping earthquakes may be biased toward pairs that are within a few magnitude units of one another, as they were initially visually identified. Even smaller magnitude events may occur nearly simultaneously or trailing larger events but were not detected or located due to poor network coverage. Enhancing earthquake detection by applying machine learning may identify several other possible overlapping events (e.g., Walter *et al.*, 2021).

Figure 10 suggests that the spatiotemporal distribution of the overlapping earthquakes indicates they predominantly occur on some of the same faults that produced large magnitude earthquakes ($M_w > 5$) or that have occurred in areas

undergoing intensive hydraulic fracturing but little wastewater disposal (e.g., Skoumal *et al.*, 2018). Almost all the overlapping earthquakes occurring between 2015 and 2017 are located on the faults that produced the $M_w > 5$ earthquakes during that period. The M_w 5.1 Fairview earthquake is sandwiched between five overlapping earthquakes, whereas three overlapping earthquakes on the M_w 5.8 Pawnee earthquake occur immediately after the main event. In Cushing two overlapping earthquakes occurred before the M_w 5.0 earthquake. The origin time difference between the main events and the accompanying overlapping earthquakes is on the scale of weeks to months suggesting that the time delay may be too large for dynamic triggering to play a role in causing the overlapping earthquakes. However, static stress transfer from the main events in the case of Fairview and Pawnee may have contributed to the overall stress change responsible for triggering these overlapping earthquakes along with far-field pore pressure and poroelasticity. These faults that reactivated to produce large magnitude earthquakes, including the Wilzetta fault that accommodated the 2011 M_w 5.7 Prague earthquake, continue to produce overlapping earthquakes within 10 km of the major event's epicenter in the 2018–2020 period. The presence of overlapping earthquakes may indicate heterogeneous or anastomosing fault zones that exhibit adjacent velocity-weakening and strengthening processes in either the preparatory or post-seismic periods but that are also capable of both aseismic slip and/or rupture in moderate earthquakes depending on the state of stress or external influencing factors.

As suggested previously, several overlapping earthquakes occur in the delineated SCOOP/STACK area-of-interest (Fig. 10), which is coincident with a recent trend of hydraulic fracturing well completions that are sometimes accompanied by earthquake swarms. The overlapping earthquakes on faults reactivated by the hydraulic fracturing process occur during the high-pressure fracturing process or the backflow period shortly after the pressure ceases. The close spatiotemporal separation of the event-pairs forming overlapping earthquakes indicates that they possibly occur on the same fault system with the possibility of being induced by either the pore-pressure perturbation or by a dynamic triggering of the second event by the preceding one while being critically stressed by the active pressurization. We plan to further study this interaction with planned future dense networks of instruments.

For a set of overlapping earthquakes, the presence of P and S shadow zones (e.g., Fig. 3) provides a challenge in identifying the second earthquake. The effect of the shadow window can vary depending on the magnitudes of the two earthquakes and the site effect at the recording station. When the magnitude of the first event is much larger than the second event, the amplitude of the P and S waves for the second event become relatively smaller, such that they become obscured by the S -wave signal and coda of the first event, making it nearly impossible to identify the second event lying in the P and S shadow zone.



On the other hand, when the first event is smaller than the second event, such that the peak amplitude of the *P* and *S* arrival for the second event is larger than the *S*-wave signal of the first event, then the shadow effect is nullified. Seismic stations located in sites underlain by unconsolidated sedimentary material experience higher site amplification than those underlain by consolidated rocks. The amplification of the coda increases the intensity duration and thereby reduces the window within which the phases from the second earthquake can be clearly identified. The combination of these factors may be limiting the detection and location of overlapping earthquakes in the region or in other regions outside of Oklahoma. It is likely that these types of events are only identifiable when the pair of event magnitudes are within a few tenths of magnitude units.

Multiphase arrivals

Crustal reverberations are commonly found in regions with low-velocity unconsolidated sedimentary layers overlaying bedrock (Langston, 2003). The high impedance contrast between the layers enables the excitation of multiple reflections and primary wave conversions. In this study, the earthquakes associated with these reverberations are primarily located in the SCOOP and STACK area for the 2019–2020 period, and the phases are observed at stations located particularly within the central region of the state (Fig. 10) as previously observed by Moschetti and Hartzell (2020).

The synthetic seismograms modeling indicates that multiphase arrivals are produced when earthquakes within the crystalline basement occur close to the top of the basement, or occur within the Paleozoic sedimentary of the Arbuckle group atop the basement. The high-impedance contrast at the boundary between Paleozoic sedimentary deposits and at the top of the crystalline basement provides a suitable condition for development of crustal reverberations. As the focal depth is placed deeper into the basement in the model, it is apparent that the amplitude of the reverberations is relatively lower. The lower

Figure 9. Spatiotemporal assessment of overlapping earthquakes, occurring between January 2019 and December 2020, for defining a universal window (a) to be used to search for overlapping earthquakes in the OGS historical catalog. (b) The temporal distribution of overlapping earthquakes in Oklahoma between January 2010 and December 2020.

amplitudes excited at the impedance contrast for deeper events are due to narrow incident angles which result in a lower reflection coefficient. The variation of the reverberation amplitude with depth has been observed in waveforms from earthquakes near Cushing, Oklahoma (Ortega Romo, 2020). The presence or absence of reverberation, as well as the associated amplitude variation, can be used to constrain earthquake focal depths in Oklahoma. Several spatial clusters of earthquakes with associated multiphase arrivals occur in proximity to “regular” earthquakes (singles). Within the SCOOP and STACK area, most of these earthquakes are induced through hydraulic fracturing processes that occur within the sedimentary layers above the basement. It is apparent that some of the earthquakes occur within the sedimentary rock units, based on the absence of multiphase arrivals, while others extend into the crystalline basement. The analyzed earthquakes have focal depths ranging between 3 and 8.7 km with a median depth of 7 km. The focal depths from the regional monitoring network are poorly constrained and, in many cases, do not conform to the observed features corresponding to shallower focal depths. We are in the process of constraining the focal depths in Oklahoma by deploying targeted Nodal surveys and using velocity models that fit the local crustal structure.

Significance of elongated duration for both types of unique events

Ground-motion duration alongside amplitude and frequency related parameters such as peak ground acceleration and spectral accelerations are key constituents in current seismic hazard

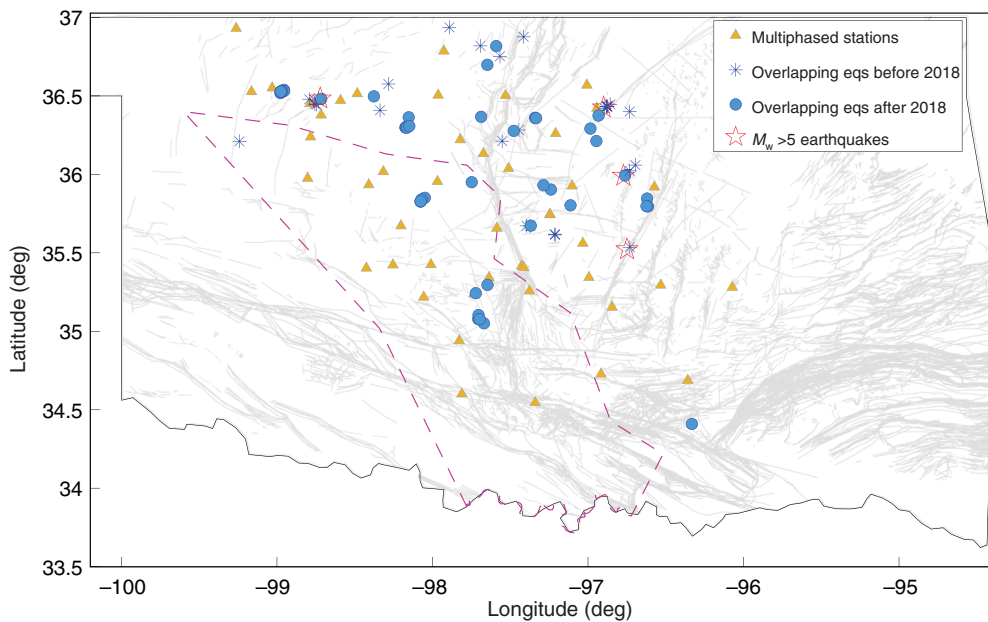


Figure 10. Spatial distribution of the overlapping earthquakes occurring between 2010 and 2017 (asterisk), and those occurring between 2018 and 2020 (circles). The large stars are the epicenters of $M_w > 5$ earthquakes in the state. The large earthquakes were not overlapping events but are provided for spatial context. The triangles (yellow) are stations with waveforms exhibiting multiphase arrivals. In the background are mapped faults in the state. The dashed line approximately traces the SCOOP and STACK area. The color version of this figure is available only in the electronic edition.

analysis and models (Bora *et al.*, 2015; Hollenback *et al.*, 2015). Although ground-motion duration parameters may not have been regarded as equally important in the geotechnical field, the ground-motion duration associated with other amplitude parameters may factor into seismic risk assessment. The number of cycles of the shaking, and by extension the ground-motion duration, has been found to directly impact the pore pressure buildup in liquefiable soils (Seed and Idriss, 1971; Green and Terri, 2005). Long-duration ground motions tend to increase the liquefaction potential of saturated sands (Idriss and Boulanger, 2006). Although liquefaction effects are common at Modified Mercalli Intensity VII, if occurring in susceptible geology, smaller accelerations associated with long-duration earthquakes may cause liquefaction where soil conditions are particularly susceptible (National Research Council, 1985). For two earthquakes of similar amplitudes, the event with a longer duration will generally be more damaging; whereas, for two events with the same energy content, it is likely that the record with a shorter duration would cause more destruction (Bommer and Martínez-Pereira, 1999). Because strong-motion duration increases with increasing earthquake magnitude, an elongated duration from a lower magnitude earthquake elevates the intensity above the expected level thereby producing equally devastating results as a higher magnitude earthquake.

Earthquakes in Oklahoma such as the September 2016 M_w 5.8 Pawnee event have produced coseismic liquefaction-induced surface deformations including fractures, sand blows, and lateral spreading (Clayton *et al.*, 2016; Kolawole *et al.*, 2017). The February 2016 M_w 5.1 Fairview earthquake produced surface deformation quantifiable through interferometric synthetic aperture radar (Barnhart *et al.*, 2018), though there was no documented evidence of liquefaction ejecta or lateral spreading cracks. The liquefaction features observed in Pawnee were mapped primarily along the unconsolidated Quaternary Alluvium and Terrace deposits. These unconsolidated deposits are common along old and current rivers that are widely spread across the state of Oklahoma (Johnson, 1983), providing favorable conditions

for liquefaction. In addition to the palpable risk of liquefiable soils, greater than expected event durations may contribute to the qualitatively elevated reported intensities for the overlapping earthquakes and events associated with multiphase arrivals.

Conclusion

We report on some unusual earthquakes in Oklahoma and describe their classification as overlapping earthquakes and events associated with multiphase arrivals based on identified phase arrivals at a local distance scale. Overlapping earthquakes occur on faults that are subjected to high-stress processes such as relatively large magnitude earthquakes and associated with the hydraulic fracturing process. The overlapping earthquakes may be more prevalent in the region but are not always locatable due to the presence of a shadow zone created by the first occurring event in a pair of overlapping earthquakes that obscures the identification of phases from the second event. Earthquakes associated with multiphase arrivals are observed in the central region of Oklahoma and produce an elongated ground-motion duration that is equivalent to the ground-motion duration from overlapping earthquakes. The combination of long duration and unconsolidated sediments provides the right recipe for liquefaction, thereby heightening seismic risk on oil and gas infrastructure such as pipelines. Future seismic hazard analysis in Oklahoma that utilizes

intensity or duration should consider the variability of ground-motion duration across the state.

We showed that, in the case of overlapping earthquakes, pairs of earthquakes that occur closely in space and time are difficult or nearly impossible to discern from the trailing event if one or the other earthquake is significantly larger. It is only with scrutiny and the serendipity of identifying earthquakes within a few tenths of magnitude units that we were able to identify the phenomena. In this article, we propose a workflow for distinguishing actual overlapping events from the more commonly observed events associated with multiphase arrivals. It is likely that such low-magnitude overlapping events occur in other regions, but their presence has not been widely documented before. Even with the implementation of machine-learning approaches to routine earthquake detection (e.g., Walter *et al.*, 2021), associators may not be able to adequately discern the occurrence of distinct events in close space and time proximity without prior consideration or careful algorithmic design. We plan to expand this analysis to attempt to identify overlapping and multiphase arrivals in other regions.

Data and Resources

The seismic data are available at the Incorporated Research Institutions for Seismology (IRIS) as archived time-series data (<http://ds.iris.edu/ds/nodes/dmc/data/types/waveform-data/>) for two networks operated by Oklahoma Geological Survey (OGS) under Federated Digital Seismic Network codes OK (doi:10.7914/SN/OK) and O2 (doi:10.7914/SN/O2). The OGS catalog is available at the OGS website (https://ogsweb.ou.edu/eq_catalog/). This article is accompanied by the supplemental material, which includes the following materials: the 2D geological model used for synthetic waveform modeling (Fig. S1); a demonstration of subtle frequency differences between S-wave signal and crustal reverberation (Fig. S2); an illustration of the correlation window test to establish the suitable window to perform correlations (Fig. S3); an example of twin earthquake identified within the set of events associated with multiphase arrivals (Fig. S4); and the final catalog of overlapping earthquakes (Table S1) and earthquakes associated with recorded multiphase arrivals (Table S2). All websites were last accessed in May 2022.

Declaration of Competing Interests

The authors acknowledge that there are no conflicts of interest recorded.

Acknowledgments

This research is partly supported by the U.S. Department of Energy, National Energy Technology Laboratory, through a contract with the Groundwater Protection Council to the Regional Induced Seismicity Collaborative (RISC) program. The authors would like to thank the two anonymous reviewers and Editor-in-Chief Allison Bent for their thorough review and constructive suggestions, which helped them improve this article considerably.

References

Arias, A. (1970). A measure of earthquake intensity, in *Seismic Design of Nuclear Power Plants*, R. Hansen (Editor), M.I.T. Press, Cambridge, Massachusetts.

- Barnhart, W. D., W. L. Yeck, and D. E. McNamara (2018). Induced earthquake and liquefaction hazards in Oklahoma, USA: Constraints from InSAR, *Remote Sens. Environ.* **218**, 1–12.
- Bohlen, T., and B. Thomas (2002). Parallel 3-D viscoelastic finite difference seismic modeling, *Comput. Geosci.* **28**, no. 8, 887–899.
- Bommer, J. J., and A. Martinez-Pereira (1999). The effective duration of earthquake strong motion, *J. Earthq. Eng.* **3**, no. 2, 127–172.
- Bora, S. S., F. Scherbaum, N. Kuehn, P. Stafford, and B. Edwards (2015). Development of a response spectral ground-motion prediction equation (GMPE) for seismic-hazard analysis from empirical Fourier spectral and duration models, *Bull. Seismol. Soc. Am.* **105**, no. 4, 2192–2218, doi: [10.1785/0120140297](https://doi.org/10.1785/0120140297).
- Brune, J. N. (1970). Tectonic stress and the spectra of seismic shear waves from earthquakes, *J. Geophys. Res.* **75**, 4997–5009.
- Clayton, P., G. Zalachoris, E. Rathje, T. Bheemasetti, S. Caballero, X. Yu, and S. Bennett (2016). The Geotechnical aspects of the September 3, 2016 M5.8 Pawnee, Oklahoma earthquake, *GEER Assoc.*, doi: [10.18118/G69885](https://doi.org/10.18118/G69885).
- Dreiling, J., M. P. Isken, and W. D. Mooney (2016). Comparison of synthetic pseudoabsolute response spectral acceleration (PSA) for four crustal regions within central and eastern North America (CENA), *Bull. Seismol. Soc. Am.* **106**, 2500, doi: [10.1785/0120160121](https://doi.org/10.1785/0120160121).
- Ellsworth, W. L. (2013). Injection-induced earthquakes, *Science* **341**, no. 6142, doi: [10.1126/science.1225942](https://doi.org/10.1126/science.1225942).
- Green, R. A., and G. A. Terri (2005). Number of equivalent cycles concept for liquefaction evaluations revisited, *J. Geotech. Geoenviron. Eng.* **131**, no. 4, 477–488.
- Holland, A. A. (2013). Earthquakes triggered by hydraulic fracturing in south-central Oklahoma, *Bull. Seismol. Soc. Am.* **103**, no. 3, 1784–1792, doi: [10.1785/0120120109](https://doi.org/10.1785/0120120109).
- Hollenback, J., N. Kuehn, C. Goulet, and N. A. Abrahamson (2015). PEER NGA-East median ground motion models, chapter 11, in *NGA-East: Median Ground Motion Models for the Central and Eastern North America Region*, PEER Report 2015/04, Pacific Earthquake Engineering Research Center, University of California, Berkeley, California, 273–309.
- Idriss, I. M., and R. W. Boulanger (2006). Semi-empirical procedures for evaluating liquefaction potential during earthquakes, *J. Soil Dynam. Earthq. Eng.* **26**, 115–30.
- Johnson, K. S. (1983). Maps showing principal groundwater resources and recharge areas in Oklahoma: Sheet 1—Unconsolidated Alluvium and Terrace deposits; and sheet 2—bedrock aquifers and recharge areas, Oklahoma State Department of Health, scale 1:500,000.
- Kempton, J. J., and J. P. Stewart (2005). Prediction equations for significant duration of earthquake ground motions considering site and near-source effects, *Earthq. Spectra* **22**, no. 4, 985–1013.
- Kolawole, F., E. A. Atekwana, and A. Ismail (2017). Near-surface electrical resistivity investigation of coseismic liquefaction-induced ground deformation associated with the 2016 Mw 5.8 Pawnee, Oklahoma, earthquake, *Seismol. Res. Lett.* **88**, 1017–1023, doi: [10.1785/0220170004](https://doi.org/10.1785/0220170004).
- Langston, C. A. (2003). Local earthquake wave propagation through Mississippi embayment sediments, part I: Body-wave phases and local site responses, *Bull. Seismol. Soc. Am.* **93**, no. 6, 2664–2684, doi: [10.1785/0120030046](https://doi.org/10.1785/0120030046).
- Lees, J. M. (1998). Multiplet analysis at Coso geothermal, *Bull. Seismol. Soc. Am.* **88**, 1127–1143.

- Moriya, H., K. Nakazato, H. Niitsuma, and R. Baria (2002). Detailed fracture system of the Soutz-sous-Forêts HDR field evaluated using microseismic multiplet analysis, *Pure Appl. Geophys.* **159**, 517–541.
- Moschetti, M. P., and S. H. Hartzell (2020). Spectral inversion for seismic site response in central Oklahoma: Low-frequency resonances from the great unconformity, *Bull. Seismol. Soc. Am.* **111**, no. 1, 87–100, doi: [10.1785/0120200220](https://doi.org/10.1785/0120200220).
- National Research Council (1985). *Liquefaction of Soils during Earthquakes*, Committee on Earthquake Engineering, National Research Council (U.S.), Washington, D.C., doi: [10.17226/19275](https://doi.org/10.17226/19275).
- OCC (2016). New Year, New Plays, New Plans, available at <https://oklahoma.gov/content/dam/ok/en/occ/documents/ajls/news/2016/12-20-16scoop-stack.pdf> (last accessed June 2022).
- Ortega Romo, A. (2020). Aspects of seismicity clustering, subsurface structure, and stress orientations, *Master's Thesis*, University of Oklahoma.
- Poupinet, G., J. Fréchet, W. L. Ellsworth, M. J. Frémont, and F. Glangeau (1985). Doublet analysis: Improved accuracy for earthquake prediction studies, *Earthq. Pred. Res.* **3**, 147–159.
- Reyes, C. G., and M. E. West (2011). The waveform suite: A robust platform for manipulating waveforms in MATLAB, *Seismol. Res. Lett.* **82**, no. 1, 104–110, doi: [10.1785/gssrl.82.1.104](https://doi.org/10.1785/gssrl.82.1.104).
- Seed, H. B., and I. M. Idriss (1971). Simplified procedure for evaluating soil liquefaction potential, *J. Soil Mech. Found. Div.* **97**, 1249–1273.
- Shemeta, J. E., C. E. Brooks, and C. C. Lord (2019). Well stimulation seismicity in Oklahoma: Cataloging earthquakes related to hydraulic fracturing, *Unconventional Resources Technology Conference (URTEC)*, Brisbane, Australia, Society for Exploration Geophysicists, 18–19 November 2019, 95–106.
- Skoumal, R. J., R. Ries, M. R. Brudzinski, A. J. Barbour, and B. S. Currie (2018). Earthquakes induced by hydraulic fracturing are pervasive in Oklahoma, *J. Geophys. Res.* **123**, no. 12, doi: [10.1029/2018JB016790](https://doi.org/10.1029/2018JB016790).
- Toth, C. R., A. A. Holland, K. Keranen, and A. Gibson (2012). Relocation and comparison of the 2010 M 4.1 and 2011 M 5.6 earthquake sequences in Lincoln County, Oklahoma, *Eastern Section SSA 2012 Annual Meeting*, Blacksburg, Virginia, 28–30 October 2012.
- Walter, J. I., P. Ogwari, A. Thiel, F. Ferrer, and I. Woelfel (2021). easyQuake: Putting machine learning to work for your regional seismic network or local earthquake study, *Seismol. Res. Lett.* **92**, 555–563, doi: [10.1785/0220200226](https://doi.org/10.1785/0220200226).
- Walter, J. I., P. Ogwari, A. Thiel, F. Ferrer, I. Woelfel, J. C. Chang, A. P. Darold, and A. A. Holland (2020). The Oklahoma geological survey statewide seismic network, *Seismol. Res. Lett.* **91**, 611–621, doi: [10.1785/0220190211](https://doi.org/10.1785/0220190211).
- Yeck, W. L., G. P. Hayes, D. E. McNamara, J. L. Rubinstein, W. D. Barnhart, P. S. Earle, and H. M. Benz (2017). Oklahoma experiences largest earthquake during ongoing regional wastewater injection hazard mitigation efforts, *Geophys. Res. Lett.* **44**, 711–717, doi: [10.1002/2016GL071685](https://doi.org/10.1002/2016GL071685).

Manuscript received 28 February 2022

Published online 15 July 2022